Available online at www.sciencedirect.com
SCIENCE DIRECT®
Journal of Sound and Vibration 286 (2005) 673–696
JOURNAL OF SOUND AND VIBRATION
www.elsevier.com/locate/jsvi

An integrated characteristic simulation method for hydraulically damped rubber mount of vehicle engine

Li-Rong Wang[a,*], Jia-Cai Wang[b], Ichiro Hagiwara[a]

[a]*Hagiwara Lab, Department of Mechanical Science and Engineering, Tokyo Institute of Technology, 2-12-1, O-okayama, Meguro-ku, 152-8522, Tokyo, Japan*
[b]*Mechatronics Research Center, School of Mechanical & Vehicle Engineering, Beijing Institute of Technology, No. 5, Zhongguancun Nandajie, Haidian District, Beijing, 100081, PR China*

Received 28 April 2004; received in revised form 27 September 2004; accepted 14 October 2004
Available online 22 January 2005

Abstract

Hydraulically Damped Rubber Mount (HDM) is widely equipped in vehicle powertrain mounting system and plays an important role in noise, vibration and harshness (NVH) control of vehicle. It is necessary that static and dynamic characteristics of HDM and its effectiveness on vibration isolation of powertrain system are predicted at design and development stage. In this paper, a kind of graphic HDM modeling method integrating with parameter identifications obtained from finite element (FE) analysis and experimental analysis is investigated to predict performance of HDM. The fluid–structure interactions in HDM are explored by predictions of volumetric elasticity and equivalent piston area of fluid chamber using a kind of hydrostatic fluid–structure FE method in commercial code of ABAQUS. Predications of static elasticity and dynamic characteristics and frequency response analysis of a typical HDM with fixed-decoupler verify the effectiveness of the proposed method. This research helps automotive engineers to enhance computer-aided system technology in design and development of HDM and powertrain mounting system.

*Corresponding author. Tel.: 81 3 5734 3630.
E-mail addresses: wanglr@mech.titech.ac.jp (L.-R. Wang), wangjc@mech.titech.ac.jp (J.-C. Wang), hagiwara@mech.titech.ac.jp (I. Hagiwara).

0022-460X/$ - see front matter © 2004 Elsevier Ltd. All rights reserved.
doi:10.1016/j.jsv.2004.10.037

1. Introduction

Nowadays vehicle powertrain mounting system (PMS) plays a more and more important role in automotive noise, vibration and harshness (NVH) control. Engine mount as the main isolator in PMS is very important to achieve good isolation performance of PMS. Hydraulically damped rubber mounts (HDM) possessing frequency- and amplitude-dependent dynamic characteristics superior to conventional elastomeric rubber mount has become a kind of effective engine mount to attenuate vibrations transmitting between powertrain and body/chassis and to reduce the interior noise of vehicle compartment. HDM is widely equipped not only in powertrain isolation system of vehicle, but also in vehicle cab mounting system, wheel suspension system, and other mobile or stationary machines' mounting systems.

Performance predictions of HDM help to explore optional schemes, ensure design quality, shorten product design cycle and reduce development cost at HDM design and development stage. Numerous articles attempted to explore modeling methods of HDM and to explain complex behaviors of HDM. Conventional method is to establish lumped parameter model of HDM, such as mechanical model [1–8] and bond graph model [9–12]. Mechanical model illustrates the mechanisms of HDM, by which engineers manually derive system equation before they make program to perform characteristic analysis. Bond graph modeling method can build up unified model for rubber and fluid parts, by which system equation can be derived by using bond graph tool or by hand. In this paper, a graphic HDM model is established from mechanical model based on a general modeling procedure for multi-domain system, in which rubber and fluid parts are modeled in a unified form, and computation can be carried out directly on the graphic model without deriving the whole system equation. Moreover, parameter identifications considering hyperelasticity of rubber material, large deformation of rubber parts and fluid–rubber interaction between rubber components and fluid in chambers are investigated to enlarge capability of performance prediction for computer-aided design of HDM. Rubber hyperelasticity and static elasticity of rubber components are taken into consideration by using a nonlinear finite element (FE) method for hyperelastic material. Fluid–rubber interactions are considered using a kind of FE analysis of hydrostatic fluid–structure interaction. Dynamic characteristics of rubber spring is measured from dynamic characteristic experiment. These parameter identifications are embedded into the proposed graphic model of HDM. Predictaions of static elasticity and dynamic characteristics and frequency response analysis of a typical HDM with fixed-decoupler are compared with experimental measurements, which verifies the effectiveness of the proposed approach. The presented modeling method of HDM bridging physical model and automatic numerical simulation can be conveniently applied in design and development of HDM to enhance capability and efficiency of computer-aided design of PMS.

2. A graphic modeling and simulation method

A graphic modeling and simulation method for multi-domain system presented in Ref. [13] is briefly introducted.

2.1. Fundamental items

The following fundamental items are used to build up the graphic modeling structure:

(1) *Effort–flow structure*: Dynamics of physical system stems from power exchange among system components. Effort and flow are the general power variables of multi-domain system, whose product is interpreted as power [14]. Power interchanged among components of physical system is described as power flow. Effort–flow modeling structure is established by two signal lines representing effort and flow in the opposite direction respectively, which enables multi-disciplinary system to be modeled in a unified format on the basis of power conservation and modeling analogies involved in various energy types.
(2) *Element unit*: There are three kinds of element units, inertia element, capacitor element and resistor element. Each of them represents the constitutive law between effort and flow, and is connected between effort–flow structures.
(3) *Connector*: There are two kinds of connectors, distribution connector and sum-to-zero connector regarded as dual connectors. At distribution connector, all signals attached to it are identical; at sum-to-zero connector, the algebraic sum of all signals attached to it is zero and there is only one output signal. Sum-to-zero connector corresponds to the general Korchhoff's current law. When an element unit is connected with effort–flow modeling structure, a dual connector pair, effort sum-to-zero pairing with flow distributor or flow sum-to-zero pairing with effort distributor, is attached to the two ends of the element unit respectively.
(4) *Transformer*: Transformer represents power transmission relationship between different energy types to keep power conservation.
(5) *Signal source*: Signal sources, including effort source and flow source, represent interaction of a physical system with the environment and supply energy input into the system.
(6) *Causality analysis*: Causality analysis is to assign computational directions of effort–flow structure and element unit. The procedure of causal analysis can be propagated as the following way. Firstly, the direction of effort and flow structure connecting to power source is assigned in positive power input direction. Secondly, directions of inertia element and capacitor element are assigned. Integration causality rather than derivative causality is recommended. One important limitation inherent in derivative algorithms is that the time step for derivative causality must be smaller than that for integral causality to achieve computational convergence and accuracy. Finally, direction of resistor element is assigned directly in compatible way with the directions of its neighbors.

2.2. Generalized modeling procedure for multi-domain system

Based on the former fundamental descriptions, a systematic procedure to generate a graphic model from multi-domain physical system is proposed. In this procedure, the modeling processes for mechanical domain and non-mechanical domain are the same; however, variable used as reference to establish effort–flow structure in non-mechanical or mechanical system is different, that is, effort is regarded as the reference variable in non-mechanical domain

and velocity as the reference variable in mechanical domain. The modeling procedures are as follows:

(1) Lumped-parameter model to describe physical property of engineering system is established, which should be simple enough if accuracy requirement of engineering is met. Different physical domains and their relative element units are identified and modeled in one subsystem, and each subsystem can be built up individually according to the following steps of 2 to 5. If a subsystem is complicated, hierarchical modeling arrangement had better be conducted to build up a legible configuration.
(2) Effort–flow structure is set up for each reference variable. In non-mechanical domain, effort–flow structure for each effort variable is set up with attachment of a connector pair of flow sum-to-zero and effort distribution; in mechanical domain, effort–flow structure for each velocity variable is built up with attachment of connector pair of force sum-to-zero and velocity distribution.
(3) Element unit and signal source connecting with the reference variables are attached to their corresponding effort–flow structure in directions assigned by causality analysis.
(4) Difference between two neighbor reference variables is taken into consideration if some element unit is relevant to it. In non-mechanical domain, a connector pair of effort sum-to-zero and flow distribution is inserted between the two neighbor effort–flow structures to indicate such difference; in mechanical domain, a connector pair of velocity sum-to-zero and force distribution is inserted. Then, element unit relating to such variable difference is attached in direction assigned by causality analysis.
(5) Transformer is inserted along the continuous power flow line. Subsystem models are encapsulated and arranged in hierarchy to assemble the entire system model.

Such modeling procedure is demonstrated by a mechanical system with 1 dof (degree of freedom) as shown in Fig. 1(a). The modeling process as shown in Fig. 1(b) is as follows:

(1) Set up three force–velocity structures for v_1, v_2 and v_3;
(2) Add force source to f_1-v_1 structure and velocity source to f_2-v_2 structure, and attach element M to f_2-v_2 structure with a connector pair of velocity distribution and force sum-to-zero;
(3) Set up three connector pairs of force distribution and velocity sum-to-zero to represent three velocity differences between v_1 and v_r, between v_2 and v_r and between v_2 and v_3, respectively. Then attach C_r, K and C_g to their corresponding velocity difference connectors respectively;
(4) Perform causality analysis to assign the directions of velocity, force and element unit, and assemble all the three force–velocity structures into an entire model;
(5) Simplify the model.

2.3. Simulation approach

Two approaches can be used to perform numerical computation of the presented graphic model. One approach is to derive system equation from the graphic model and to perform computation of the equation; nevertheless, it is necessary to have a special tool to translate the graphic model into system equation. The other method is to carry out computation directly on

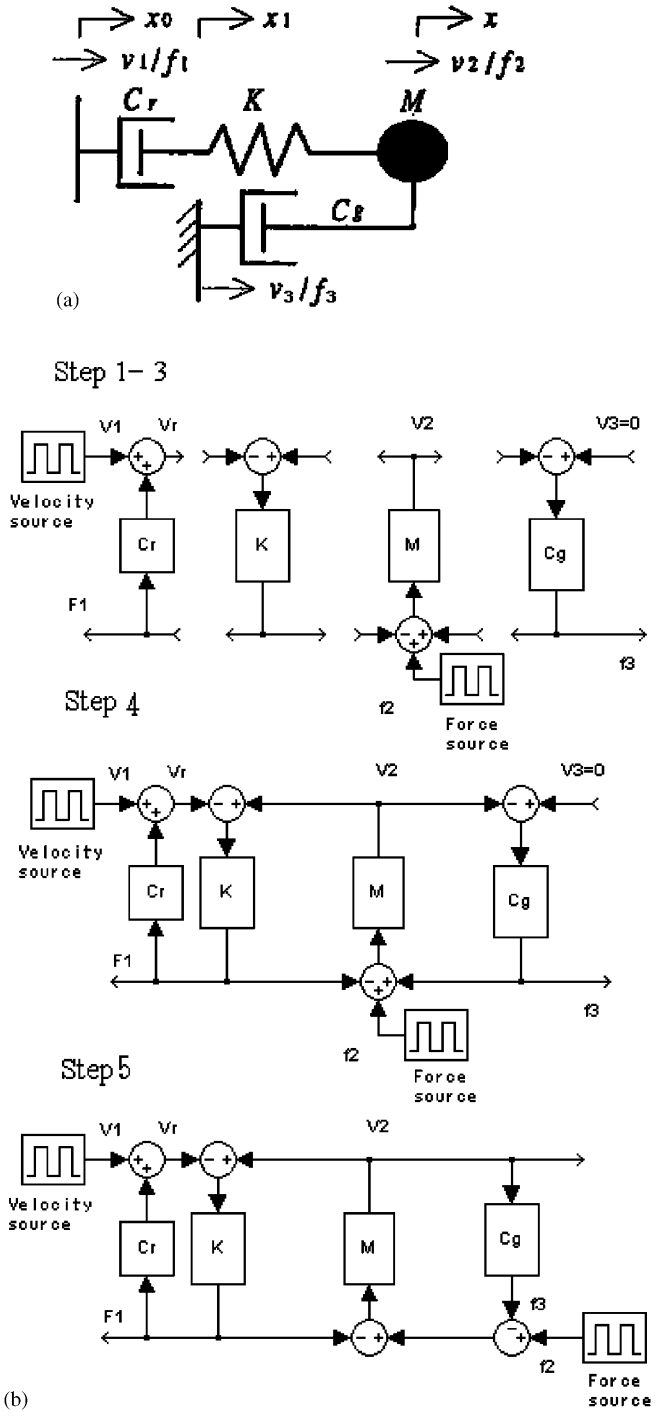

Fig. 1. A mechanical system. (a) Physical model, (b) modeling process with integral causality analysis.

graphic model without deriving system equation. In this method, block-based numerical method is adopted and calculation is performed block by block at each time step. This paper is to investigate the second approach by using the commercial code of Simulink [15]. Advantages of adopting Simulink are as follows: capabilities of Simulink to solve algebraic-loop relevant to both differential-algebraic equation (DAE) and ordinary differential equation (ODE) help to work out general engineering problems; new component library can be developed by using *S*-Functions, Matlab program or C program; hierarchical model can be constructed by using encapsulated subsystem to improve reusability of subsystem and understandability of complex model; combination with block diagram model set up from mathematic equation improves modeling flexibility for complicated system; analysis and design methods like experimental analysis and optimization design are also readily incorporated by using Matlab toolboxes.

3. Graphic model of HDM

3.1. Structure of HDM

A typical HDM used in a vehicle powertrain system is chosen for this study. Fig. 2 shows the structure of the HDM, which is mainly composed of a rubber spring, two fluid chambers, a fluid track and a decoupler membrane. Rubber spring possessing high elasticity serves as main support of powertrain load and as a piston to pump fluid to flow between upper and lower chambers through fluid track. The main physical property of rubber spring is characterized by its elastic stiffness and damping. Fluid track plays a role as tuned isolator damper. Subsystem consisting of fluid inertia in fluid track and volumetric elasticity of upper chamber results in nonlinear

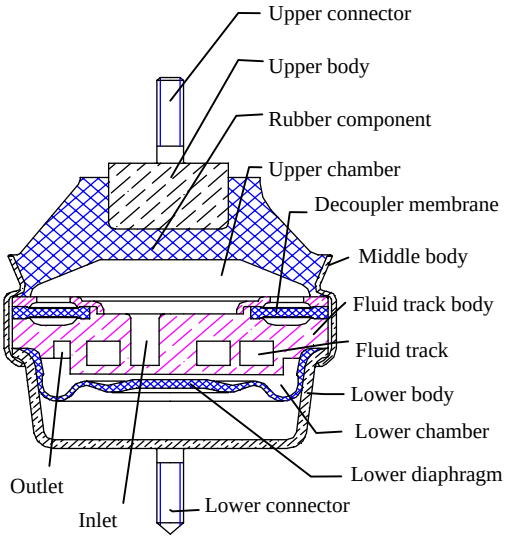

Fig. 2. Structure of HDM.

frequency- and amplitude-dependent isolation performances of HDM, which provides large dynamic stiffness and higher damping to isolate low-frequency and large-amplitude vibration effectively. Decoupler membrane helps to increase volumetric elasticity of upper chamber to achieve good isolation for high-frequency and small-amplitude vibration when there is less fluid flowing between chambers.

3.2. Models of HDM

Lumped-parameter model of HDM is set up based on the following assumptions:

- Fluid is incompressible, and fluid density in chambers and fluid track is the same.
- Pressure in chambers and fluid track is treated as hydrostatic pressure and pressure gradient is negligible. Fluid inertia and damping in upper and lower chambers are also ignored.
- Mass of rubber spring, lower diaphragm, decoupler membrane, and upper and lower connectors are negligible.
- Damping of both lower diaphragm and decoupler membrane are negligible.
- Leakage path tending to short-circuit fluid track is ignored.

Figs. 3(a) and (b) show the mechanical models and bond graph model. These lumped-parameter models include three subsystems: one is composed of elastic stiffness K_r and damping C_r of rubber spring; the second one is oscillatory system composed of fluid inertia I_f and volumetric stiffness K_{up} (called inertia track subsystem); the third one is the accumulator subsystem of lower chamber represented by volumetric stiffness of K_{low}. When excitation presses upper connector, K_r and C_r respond with reaction force upon upper connector, at the same time, fluid in upper chamber pumped by rubber spring reacts with fluid pressure upon rubber spring. The piston pump effect of rubber spring is equivalent to a cylinder piston with cross section of A_p called equivalent piston area, that is, fluid volume pumped by rubber spring is equivalent to that pumped by the cylinder piston. One part of fluid displaced by rubber spring flows into lower chamber, and the other part bulges rubber spring and increases fluid volume in upper chamber. Due to softness of lower diaphragm, fluid pressure in lower chamber is almost the same as the atmosphere outside of lower diaphragm.

A graphic model of HDM is shown in Fig. 3(c), which is built up according to the following procedures:

(1) Force–velocity structure is built up for rubber spring subsystem, and pressure–volume flow rate structure for inertia track subsystem. Element units of K_r and C_r are attached to force–velocity structure by connectors of force sum-to-zero and velocity distribution respectively, and element units of I_f and R_f are attached to pressure–volume flow rate structure by connectors of pressure sum-to-zero and volume flow rate distribution.
(2) Two pairs of connectors of volume flow rate sum-to-zero and pressure distribution are attached to pressure–volume flow rate structure of fluid track, and the corresponding element units of K_{up} and K_{low} are added.
(3) Transformer block of equivalent piston area A_p is inserted between force–velocity structure and pressure–volume flow rate structure to represent the power exchange between rubber component subsystem and inertia track subsystem.

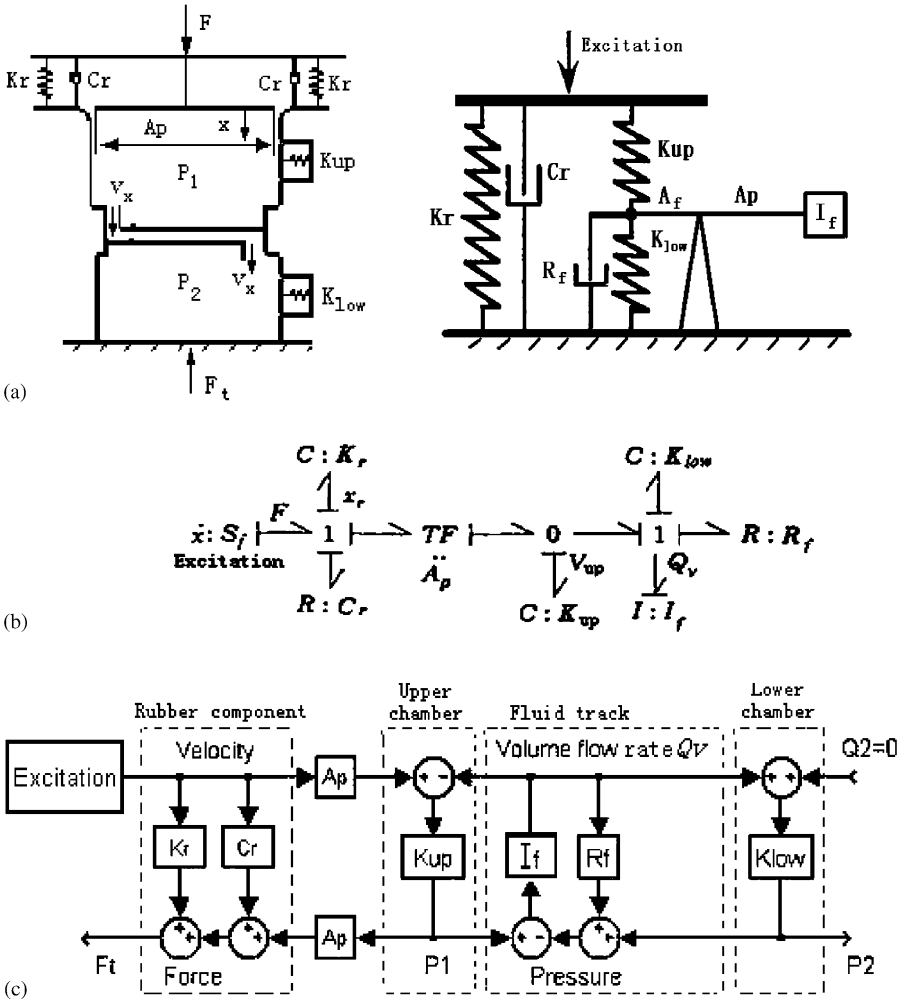

Fig. 3. HDM models. (a) Mechanical models, (b) bond graph model, (c) Graphic model.

(4) Element units are created by using *S*-Function according to parameter identifications to be introduced in the next section.

Advantages of this graphic model of HDM are as follows:

- The graphic effort–flow structure builds mechanical and hydraulic subsystems in a unified format to illustrate the interaction between rubber and fluid parts and to demonstrate power flow transmitted among them, which helps to gain insight into the working mechanism of HDM at a glance of the model.
- Parameter identifications obtained from other analysis methods like experimental analysis, analytical analysis and FE analysis can be conveniently embedded in element units. Model modification and reanalysis can be carried out directly on the graphic model.

- Static and dynamic characteristics and frequency response analysis of HDM can be automatically carried out on the model with no need to derive whole system equation. Numerical results of each variable can be observed online or exported into data file. Thus, users are able to concentrate on modeling decisions and analysis of computational results without burden for deriving system equation and making numerical computation program.

4. Identification of parameter property

Accurate identifications of parameter properties considering the nonlinearities of hyperelasticity and viscoelasticity of rubber material, large deformation of rubber parts and fluid–rubber interaction between rubber components and fluid in chambers are essential to the accuracy of HDM model. Up to now, parameter identifications have been investigated by experimental measurement and computer-aided simulation method. Singh et al. investigated nonlinear properties of chamber volumetric stiffness and fluid track resistances by using experimental and analytical approaches [1]. Kern et al. predicted static elasticity of rubber components by using FE method [5]. Colgate et al. estimated chamber volumetric stiffness via frequency response experiment and analytical formula, and measured elasticity and equivalent piston area of rubber component by experiments [10]. Shibayama et al. predicted fluid track resistance by using CFD code [16]. In this section, parameter identifications obtained from FE analysis for hyperelastic material, FE analysis for hydrostatic fluid–structure interaction and experimental analysis are adopted and embedded into the proposed graphic model of HDM.

4.1. Constitutive law of rubber hyperelasticity

Constitutive law of rubber hyperelasticity as the fundamental property of rubber component is determined by FE method as presented in Ref. [17]. Firstly, uniaxial tension and compression tests of rubber specimens were carried out. Then, tension and compression test simulations with a one-element model and FE models of experimental specimen were carried out, and the suitable constitutive laws of rubber hyperelasticity are selected. At last, candidate constitutive laws of rubber material hyperelasticity were obtained based on comprehensive evaluations between simulational results of FE analysis under real working condition and experimental results. The finally determined strain energy function of each rubber material in the HDM is listed in Table 1.

Table 1
Property of rubber material

	Rubber spring	Decoupler membrane	Lower diaphragm
Form of strain energy function	Money–Rivlin	Neo-Hookean	Money–Rivlin
Coefficients in stain energy function (MPa)	$C_{10} = 0.409016$ $C_{01} = -0.019916$	$C_{10} = 0.35455$	$C_{10} = 0.241209$ $C_{01} = 0.68946$
Density (kg/m^3)	1.11×10^3	1.18×10^3	1.098×10^3

4.2. Elasticity of rubber spring

Static elasticity K_r of rubber spring is predicted by FE-based static elasticity simulation of vehicle rubber mount [18], as shown in Fig. 4. It is difficult to describe accurately nonlinear time-dependent viscoelasticity for finite deformation rubber material by using existed commercial softwares. Therefore, dynamic characteristic experiment of rubber spring is carried out by using the same HDM with no fluid on an electrohydraulic material testing system of SCHENCH HYDROPLUS [19]. The dynamic characteristics of K_r and C_r analyzed from the measured excitation displacement and reaction force of upper connector are shown in Fig. 5.

4.3. Prediction of chamber volumetric elasticity

Chamber volumetric stiffness is usually used as evaluation of chamber volumetric elasticity of fluid chamber. Volumetric stiffness of upper chamber can be expressed as $K_{up} = \Delta p_{up}/\Delta V_{up}$, where Δp_{up} and ΔV_{up} are the changes of fluid pressure and fluid volume in upper chamber, respectively. The volumetric stiffness of lower chamber K_{low} can be defined in the same way. In order to estimate chamber volumetric elasticity of K_{up} and K_{low}, FE method of hydrostatic fluid–structure interaction in commercial code of ABAQUS is adopted to describe the interactions between rubber parts and fluid in chambers. Hydrostatic FE models of upper and lower chambers of HDM are developed using PATRAN, and numerical calculations are carried out using ABAQUS/Standard Version 5.8 on a supercomputer SGI Origin 2000.

4.3.1. Finite element method of hydrostatic fluid–structure interaction

In ABAQUS, hydrostatic fluid element and 2-node fluid link element can be used to modeling fluid–filled cavity under the assumption of constant cavity pressure. Hydrostatic fluid element is

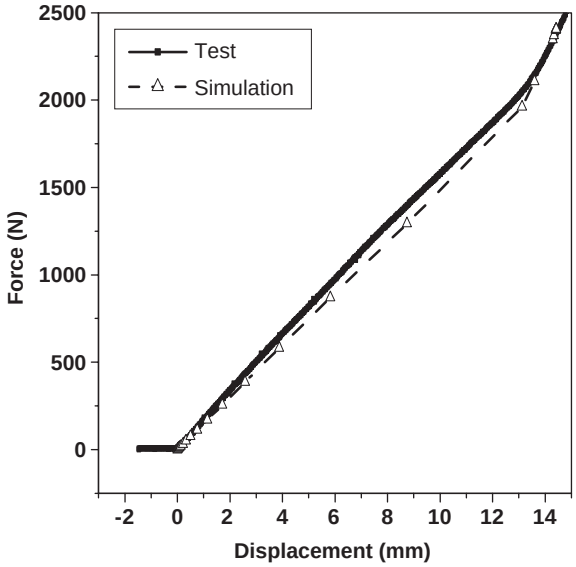

Fig. 4. Comparison of predicted vertical static elastic characteristic with experimental result.

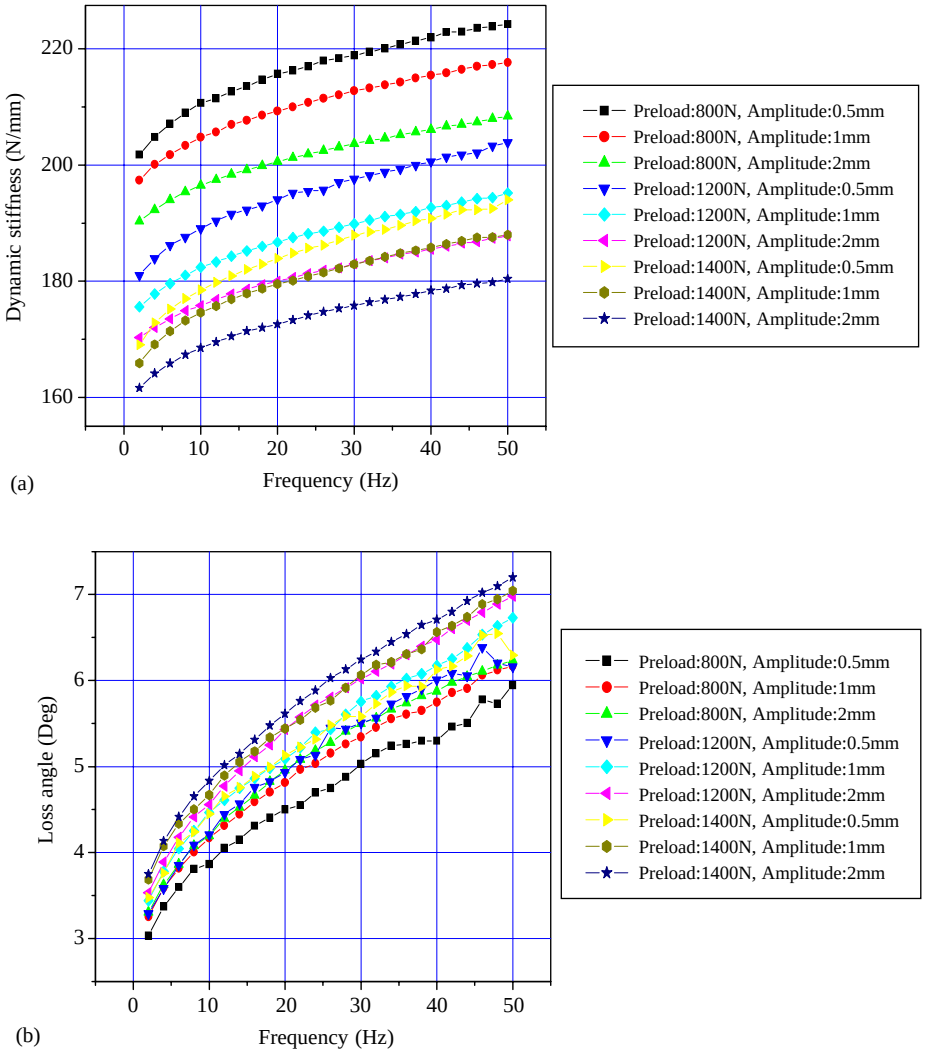

Fig. 5. Experimental results of dynamic characteristics of rubber spring. (a) Dynamic stiffness, (b) loss angle.

surface element that covers the boundary of fluid cavity to describe the coupling between deformation of fluid–filled structure and pressure of the contained fluid. Standard structure element is used to mesh fluid–filled structure. Hydrostatic fluid element and structure element shares the same nodes on the fluid–structure interface. All hydrostatic fluid elements in one cavity associate with a given node known as cavity reference node. Cavity reference node has a single dof representing fluid pressure inside the cavity. Hydrostatic fluid element is actually volume element, that is, the solid geometry constructed by the surface of a fluid element and cavity reference node is used to calculate volume of the fluid element. The sum of all the volumes of fluid elements is the actual cavity volume. On the other hand, fluid volume can also be given as a function of fluid pressure, fluid temperature and fluid mass in cavity. Volume $\tilde{V}$ derived from this function should equal to the actual cavity volume V, that is, the constraint equation $V - \tilde{V} = 0$ should be

satisfied. Therefore, FE formulation of such hydrostatic fluid–structure interaction can be achieved by augmenting the virtual work expression of the structure with this constraint equation. The virtual work contribution due to the cavity pressure can be expressed as

$$\delta\Pi^* = \delta\Pi - p\delta V - \delta p(V - \bar{V}), \tag{1}$$

where $\delta\Pi^*$ is the augmented virtual work expression, $\delta\Pi$ the virtual work expression of the structure without the cavity, p the cavity pressure. Eq. (1) represents a mixed FE formulation in which the structural displacements and fluid pressure are the primary variables. The solution of such mixed formulation can obtain the structural displacement and fluid pressure simultaneously.

In addition, when problem involves multiple fluid cavities with potential transfer of fluid between the cavities due to pressure difference between the cavities, fluid link element connecting cavity reference nodes between two cavities can describe fluid flow transferred between two cavities or between a cavity and the outside world by defining a homogeneous function expressing relationship between mass flow rate and pressure difference. It is assumed that fluid in both cavities is the same, but pressure in each cavity may be different. The mass change integrated over a finite increment using the mass flow rate function needs to be converted into volume change in each cavity. Then solving the mixed formulation of each cavity individually shown in Eq. (1), the structural displacement and fluid pressure of each cavity are obtained. There are two methods to define a function between mass flow rate and the pressure difference. One method is defined by equation expressed as

$$Q_m = C_V \Delta p + C_H \Delta p|\Delta p|, \tag{2}$$

where Q_m is mass flow rate, Δp the pressure difference, C_V the viscous resistance coefficient, and C_H the hydrodynamic resistance coefficient. Another method is to specify a user-defined table of mass flow rate versus pressure difference.

4.3.2. *Prediction of volumetric elasticity of upper chamber*

As shown in Fig. 6, an axisymmetric FE model of upper chamber is set up by cutting down lower chamber and part of fluid track body and neglecting some minor non-axisymmetric features of the outer part of rubber spring. CAX4H element (4-node bilinear, hybrid element with constant pressure) is selected to mesh rubber spring and decoupler membrane. CAX4 element (4-node

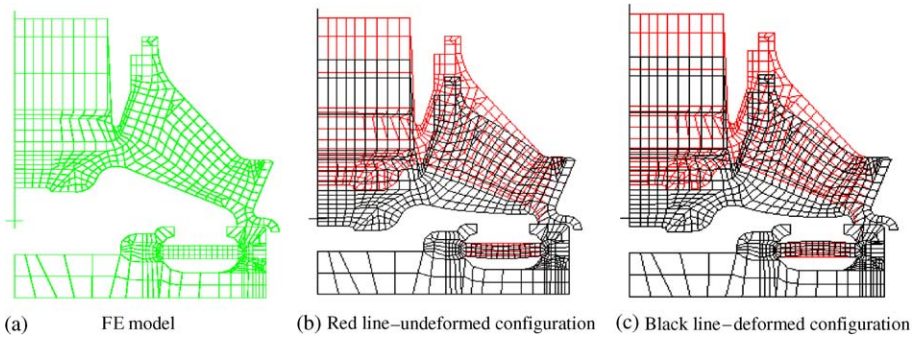

Fig. 6. FE model for prediction of volumetric elasticity of upper chamber. (a) FE model, (b) fluid is injected into upper chamber, (c) fluid is extracted from upper chamber.

bilinear element) is used to mesh fluid track body, upper body, middle body, and metal reinforcing part in rubber spring. An additional rigid body as a loading head is defined to contact with the top end of upper body and given a vertical loading displacement to the reference node of the rigid body. The bottom suface of fluid track body is fixed, and the middle body is truncated and fixed at the bottom face.

FAX2 element (2-node linear hydrostatic fluid element) is choosen to model upper chamber. All the fluid elements cover the entire fluid–structure interfaces of upper chamber, and share the same nodes with the structure elements of rubber spring, decoupler membrane and fluid track body on the fluid–structure interface. A cavity reference node is defined on the model's symmetry axis, and is placed in the middle between the intersection point of the axis passing through the interior surface of rubber spring and the intersection point of the axis passing through the top surface of fluid track when no deformation occurs in the model. Fluid density and pressure is specified to this cavity reference node. Fluid pressure in upper chamber according to the simulation results of static characteristic of HDM has to be prescribed corresponding to the real working state of HDM under the preload of engine in order to assure proper calculation of the cavity volume, because prescribing the pressure at the cavity reference node is equivalent to applying a uniform pressure on the cavity boundary. Another cavity reference node is defined on the model's symmetry axis outside of upper chamber. Thus, a fluid link element can be defined by connecting the two reference nodes. A prescribed quantity fluid can be added into or removed from the chamber by specifying mass flow rate to the cavity reference node in the upper chamber. A positive mass flow rate adds fluid into cavity, while a negative mass flow rate removes fluid from cavity. Furthermore, three pairs of slave–master contact surfaces are defined: one contact pair is that the interior surface of rubber spring is prescribed as slave contact surface, and the top surface of fluid track body is prescribed as master contact surface; the second contact pair is that the top face of decoupler membrane is prescribed as slave contact surface, and the surface of fluid track body possible to contact with top face of decoupler membrane is prescribed as master contact surface; the third pair is that the bottom face of decoupler membrane is prescribed as slave contact surface, and the surface of fluid track body possible to contact with the bottom face of decoupler membrane is prescribed as master contact surface. This axisymmetric model has 848 elements, 1389 nodes and 2158 dofs.

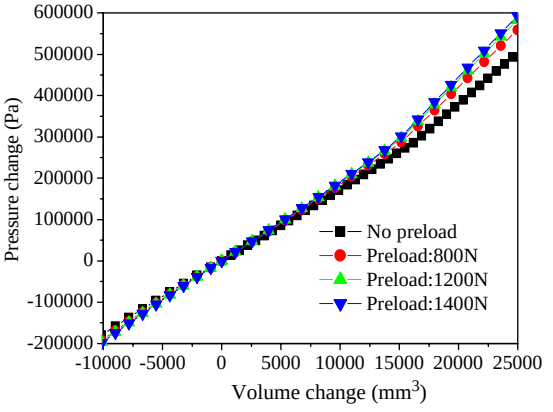

Fig. 7. Predicted volumetric elasticity of upper chamber.

Table 2
Predicted volumetric stiffness of upper chamber

Preload (N)	Volumetric stiffness (N/(mm)^5)			
	None	800	1200	1400
Fluid is added into chamber				
No contact between decoupler membrane and fluid track	17.36	18.68	19.16	19.34
Contact between decoupler membrane and fluid track	23.69	27.35	28.99	29.73
Fluid is removed from chamber	17.96	20.20	20.66	19.91

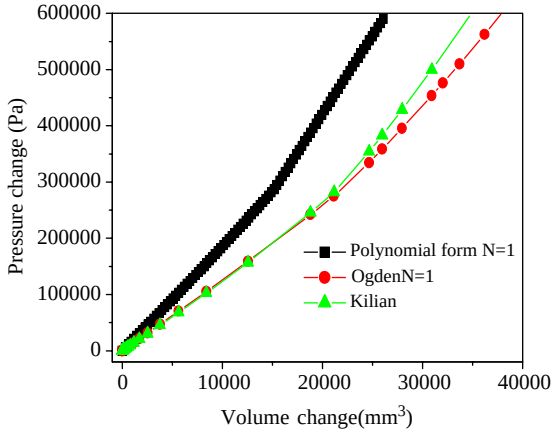

Fig. 8. Predicted volumetric elasticity of upper chamber with various constitutive law for rubber spring under preload of 800 N.

Volumatric elasticity of upper chamber is predicted when a prescribed quantity of fluid is added into or removed from chamber, as shown in Fig. 7. The calculated volumetric stiffness of upper chamber is listed in Table 2. The volumetric elasticity of upper chamber when adopting various rubber constitutive laws for rubber spring is shown in Fig. 8. These predicted results demonstrate the following points:

- When fluid is added into chamber, volumetric elasticity of upper chamber shows stage linearity. After volume change is larger than 15,000 mm^3, decoupler membrane contacts with fluid track body, and volumetric elasticity becomes harder. When fluid is removed out of chamber, volumetric elasticity shows linearity.
- Volumetric elasticity shows a little preload-dependent characteristic, that is, volumetric elasticity becomes harder when preload is increased, and such preload-dependent characteristic decreases with increase of preload.
- Rubber hyperelasticity for rubber spring has great influence on volumetric elasticity of upper chamber, which indicates that the accuracy of constitutive law of rubber component is essential to the accuracy of the prediction volumetric elasticity.

4.3.3. Prediction of equivalent piston area

Prediction of equivalent piston area A_p can also be performed on the FE model shown in Fig. 6. when filling air into chamber instead of fluid and connecting the chamber air with the atmosphere by prescribing the atmosphere density and pressure to the reference node outside of the chamber. Characteristic of equivalent piston area can be evaluated by the relationship between air volume change in upper chamber and the vertical loading displacement pressed to the loading head, because the air volume change pumped by rubber spring under the loading displacement is equivalent to the air volume pumped by cylinder piston. The predicted equivalent piston area shown in Fig. 9 illustates that equivalent piston area A_p shows nonlinearity before rubber spring contacts with fluid track body. A_p decreases sharply after rubber spring contacts with fluid track body due to little volume change of upper chamber. Such property of A_p is reasonable to the real working state of HDM. HDM seldom works in the state of rubber spring contacting with fluid track body. Therefore, the predicted A_p before contact occurs is adopted in performance simulation of HDM shown in next section.

4.3.4. Prediction of volumetric elasticity of lower chamber

As shown in Fig. 10, an axisymmetric FE model of lower chamber is set up by cutting down upper chamber and part of fluid track body. CAX4 H element is selected to mesh the lower diaphragm. CAX4 element is used to mesh the lower body and fluid track body. The bottom surface of lower body and the top suface of fuid track body are fixed respectively. FAX2 element is choosen to model the fluid–filled lower chamber. All the fluid elements cover the entire fluid–structure interfaces, and share the same nodes with the structure elements of lower diaphragm and fluid track body on the fluid–structure interfaces. A cavity reference node is defined on the model's symmetry axis, and is placed in the middle between the intersection point of the axis passing through the top surface of low diaphragm and the intersection point of the axis passing through the bottom face of track body when no deformation occurs in the model. Fluid density, pressure and mass flow rate is specified to the cavity reference node. Moreover, two pairs

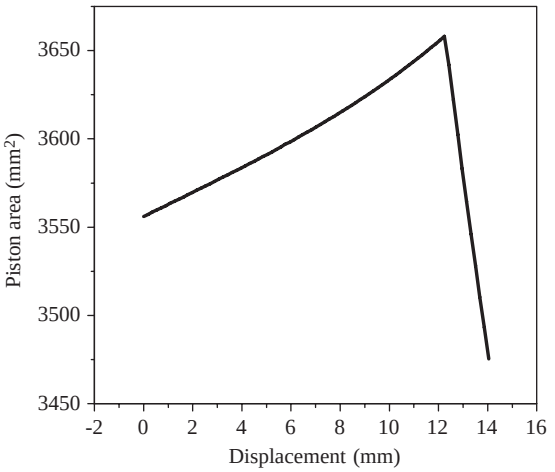

Fig. 9. Predicted equivalent piston area of A_p.

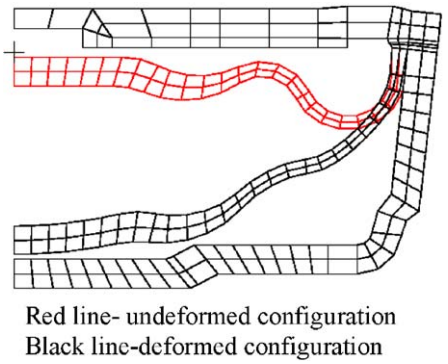

Fig. 10. FE model for prediction of volumetric elasticity of lower chamber.

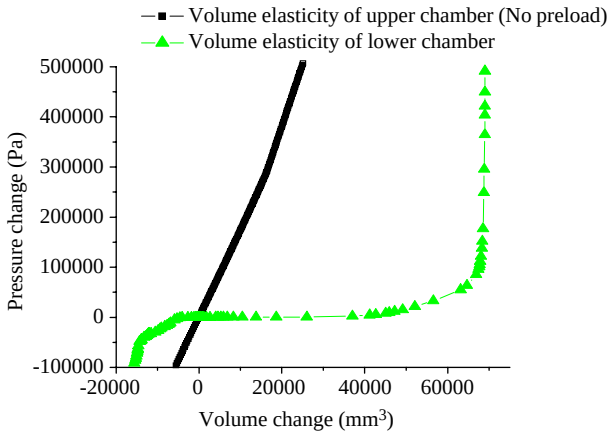

Fig. 11. Predicted volumetric elasticity.

of slave–master contact surfaces are defined: one contact pair is that the top face of lower diaphragm is prescribed as slave contact surface, and the bottom face of fluid track body is prescribed as master contact surface; the other contact pair is that the bottom face of low diaphragm is prescribed as slave contact surface, and the top face of lower body is prescribed as master contact surface. This axisymmetric model has 148 elements, 267 nodes and 381 dofs.

The predicted volumetric elasticity of lower chamber, as shown in Fig. 11, demonstrates that the volumetric stiffness of lower chamber keeps soft property, but it increases sharply when low diaphragm contacts with the fluid track body or lower body. In real working conditions, the volume designs of upper and lower chambers ensure that lower diagram cannot touch the lower body even though all the fluid in upper chamber is driven into the lower chamber, and it is impossible to drive all the fluid in the lower chamber into the upper chamber. Hence, volumetric elasticity of lower chamber before the contact occurs is adopted in performance simulation of HDM shown in next section. Comparison between volumetric stiffness of upper and lower chambers when no contact occurs, as shown in Fig. 11, illustrates that volumetric

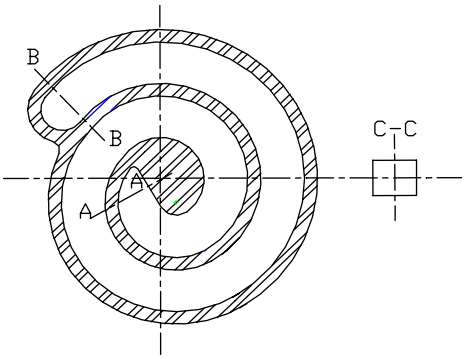

Fig. 12. Mechanical model of fluid track.

stiffness of lower chamber is much softer than that of upper chamber. Therefore, the influence of the volumetric elasticity of lower chamber on the characteristic of HDM can almost be neglected.

4.4. Parameters associated with hydraulic system

Fluid inertia I_f in the fluid track plays a significant role in frequency- and amplitude-dependent characteristics of HDM, and its accurate estimation is essential to the accuracy of predicted dynamic characteristic. Fluid inertia I_f can be expressed as $I_f = \rho L/A$, where ρ is fluid density, L and A are the length and cross area of fluid track respectively. Geometrical dimension of fluid track is obtained according to the 3D geometrical model of fluid track. Fluid density is measured by physical property experiment.

Fluid resistance R_f is dynamically calculated according to the fluid flow state in fluid track. Fluid dynamic characteristic in fluid track is studied based on fluid mechanics model shown in Fig. 12. The fluid mathematical model established according to Bernoulli Equation [20] can be expressed in mass flow rate format as

$$\dot{Q}_m + \frac{1}{2\rho AL}\left(\frac{fL}{D_h} + \xi\right) Q_m^2 \,\mathrm{sign}(Q_m) = \frac{A}{L}\,\Delta p, \tag{3}$$

where p_1 and p_2 are average pressure on the section A-A and section B-B, respectively; $\Delta p = p_1 - p_2$ the pressure difference between inlet and outlet of fluid track; the mass flow rate $Q_m = \rho \mathrm{A} v_x$, here v_x is the flow velocity along fluid stream line; and sign the sign function. Fluid resistance $R_f = \frac{1}{2}(f_l L/D_h + \xi)v_x^2$ includes major loss and minor loss of fluid track, where ξ is minor loss coefficient, which includes contraction loss coefficient of inlet $\xi_{11} = \frac{1}{2}(1 - A_{\mathrm{out}}/A_{\mathrm{in}})$, expansion loss coefficient of outlet $\xi_{12} = \frac{1}{2}(A_{\mathrm{out}}/A_{\mathrm{in}} - 1)$, and track bend loss coefficient determined by curvature radius and diameter of fluid track according to the empirical formulas [21], here A_{in} and A_{out} are the cross area of inlet and outlet respectively; f_l major loss coefficient, which is dynamically estimated according to analytical formulas listed in Table 3. The fluid flow state is evaluated by Reynold number, and the relationship between f_l and Reynold number is obtained from the formulas in Table 3, as shown in Fig. 13.

Table 3
Major loss coefficient

Fluid state	R_e	Major loss coefficient f_1
Laminar flow	$R_e \leqslant 2000$	$f_l = \frac{64}{R_e}$
Transition region	$2000 < R_e \leqslant 4000$	$f_l = \frac{(f_{l1}-f_{l2})}{2000} R_e + 2f_{l2} - f_{l1}$ $f_{l2} = \frac{64}{R_1}, f_{l1} = \left[-2\log_{10}\left(\frac{\delta}{3.7} + \frac{2.51}{4000\sqrt{f_{l1}}}\right)\right]$
Turbulence flow (1)	$4000 < R_e \leqslant 5000/\delta$	$\frac{1}{\sqrt{f_l}} = -2\log_{10}\left(\frac{\delta}{3.7} + \frac{2.51}{R_e\sqrt{f_l}}\right)$
Turbulence flow (2)	$5000/\delta < R_e$	$f_l = \text{constant}$

Note: $R_e = \frac{v_x D_h}{\mu}$ is Reynold number, where, μ is the kinematic viscosity, $D_h = 4A/L_h$ the hydraulic radius of cross section of fluid track, L_n the wet periphery, $\delta = K_s/D$ the relative roughness, K_s the equivalent roughness determinted by pipe material.

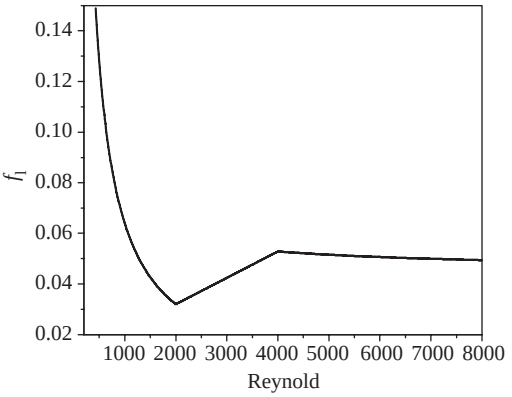

Fig. 13. f_1 versus Reynold number.

5. Characteristic predictions of HDM

5.1. Static elastic characteristic prediction

Simulation of static working process of HDM is investigated on the graphic model of HDM shown in Fig. 3(c), in which block K_r is built up according to the static elasticity prediction of rubber spring shown in Fig. 4 and block C_r is neglected. A quasi-static loading process with a slow vertical displacement loading $X_0 = X_1 \cos(0.1\pi t) - X_1$ upon the top surface of upper connector is built into an excitation block. The displacement loading and predicted vertical reaction force of upper connector are displayed in Fig. 14(a) and (b). The predicted vertical elasticity of 155.36 N/mm shown in Fig. 14(c) fits well with the experimental result, which verifies the effectiveness of the proposed method for static characteristic simulation. The predicted chamber pressure shown in Fig. 14(d) is close to atmosphere, and the predicted volume flow rate and fluid volume passing through fluid track shown in Fig. 14(e) and (f) are much few, which agree with the real working state of HDM.

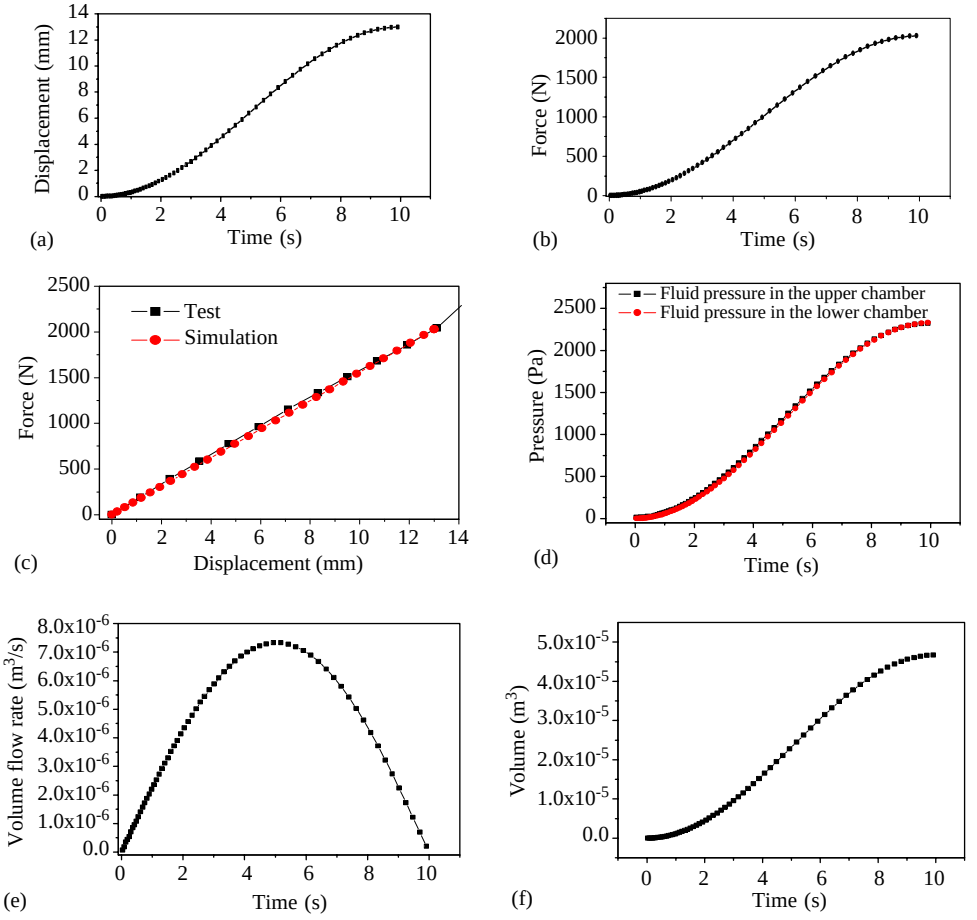

Fig. 14. Predicted static characteristics of HDM. (a) Displacement excitation, (b) reaction force, (c) vertical static elasticity, (d) fluid pressure in chambers, (e) volume flow rate through fluid track, (f) fluid volume passing through fluid track.

5.2. Dynamic characteristic prediction

Simulation of dynamic working process of HDM under harmonic loading is investigated on the graphic model of HDM shown in Fig. 3(c), in which blocks of K_r and C_r are created according to experimental results of Fig. 5. Harmonic vertical displacement of $x = X\ \cos(2\pi ft) - X$ built into an excitation block is added upon the deformed HDM under the quasi-static displacement loading of X_0. The predicted reaction forces of upper connector under various excitation frequencies are compared with the experimental results as shown in Fig. 15, in which the time axle of experimental reaction force is moved in order to compare response period and amplitude of reaction forces. Comparisons of predicted and experimental reaction forces at the frequency of 5, 10 and 16 Hz illustrate that the relative errors of amplitude are in permission range of engineering, which proves the effectiveness of this dynamic characteristic analysis method of HDM in such frequency range. However, at the higher frequency rang around 50 Hz, the amplitude difference

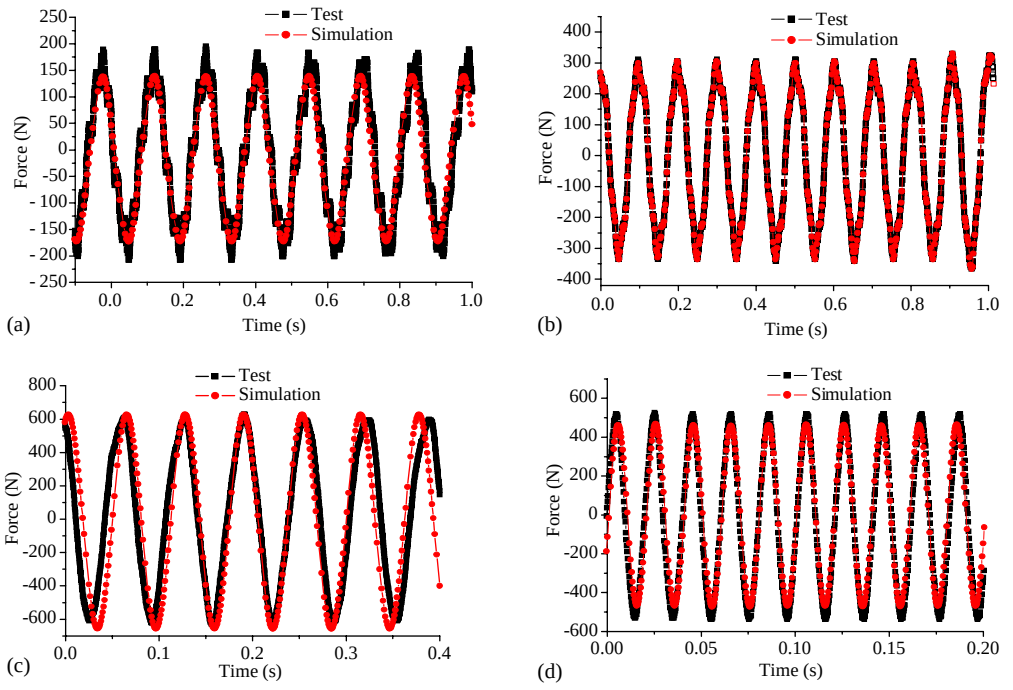

Fig. 15. Comparisons between experimental and predicted results of reaction force under preload of 800 N and harmonic excitation amplitude of 1 mm. (a) Frequency of 7 Hz, (b) frequency of 10 Hz, (c) frequency of 16 Hz, (d) frequency of 50 Hz.

between predicted force and experimental measurement becomes large. The reason will be explained in next section. As shown in Fig. 16, fluid pressure in upper chamber demonstrates frequency-dependent characteristic and fluid pressures in lower chamber keep low, which are reasonable to the real working state of HDM under corresponding boundary conditions. Fig. 17, also illustrates frequency-dependent characteristic of fluid volume flow rate passing fluid track, that is, the amplitude of volume flow rate increases with frequency, reaches the peak around 10 Hz and then decreases with the increase of frequency, which are also in accord with the actual working state of HDM.

5.3. *Frequency response analysis*

In automotive industry, frequency- and amplitude-dependent behavior of HDM is conventionally evaluated by dynamic stiffness and loss angle, which can be obtained by frequency response analysis. In frequency response analysis, complex stiffness K^* is defined as

$$K^* = \frac{F(\mathrm{j}\omega)}{X(\mathrm{j}\omega)} = K_s(\omega) + \mathrm{j}\omega C(\omega), \tag{4}$$

where $F(\mathrm{j}\omega)$ and $X(\omega)$ are the Fourier transforms of reaction force of $F(t)$ and displacement excitation of $X(t)$ under a certain loading frequency; the real part of K^* represents the elastic

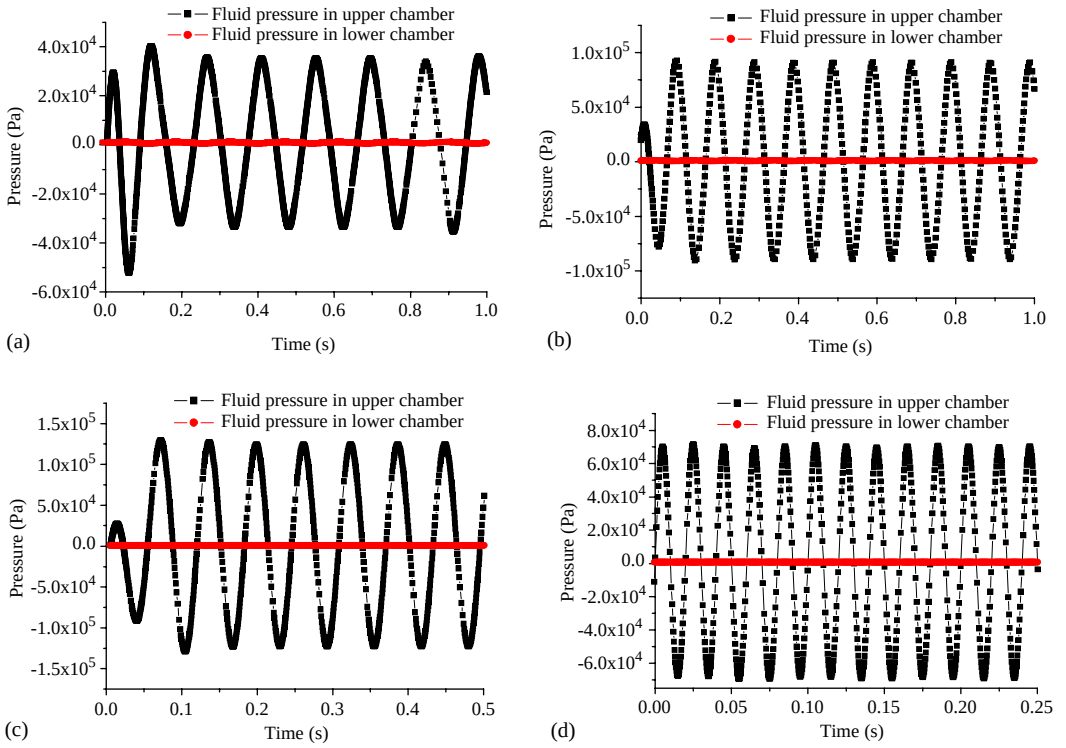

Fig. 16. Predicted results of fluid pressure under preload of 800 N and harmonic excitation amplitude of 1 mm. (a) Frequency of 7 Hz, (b) frequency of 10 Hz, (c) frequency of 16 Hz, (d) frequency of 50 Hz.

characteristic and the imaginary part divided by frequency represents the damping characteristic. Amplitude of K^* is called dynamic stiffness K_d to describe elastic property, and the phase of K^* is termed as loss angle θ_i to indicate damping property. The former predicted dynamic characteristics of HDM can be implemented into frequency response analysis.

Fig. 18 shows the analyzed dynamic stiffness and loss angle characteristics under typical working condition, which illustrates frequency- and amplitude-dependent characteristics of HDM. In low frequency range and around resonance frequency of inertia track subsystem of 10 Hz, the predicted dynamic stiffness and loss angle meet well with experimental results. Isolation performance of HDM especially the damping characteristic in the frequency range lower than 30 HZ is very important to isolation performance of PMS to effectively isolate low-frequency and large-amplitude vibrations induced by the road or the engine at idle. The proposed characteristic simulation method of HDM can reveal frequency- and amplitude-dependent characteristics of HDM in the low frequency range especially in the frequency range near to the maximum damping frequency, which prove that such method is an effective method to be applied in designs of HDM and PMS. However, in the frequency range higher than resonance frequency of inertia track subsystem, the difference between the analyzed and experimental results becomes large especially for those of dynamic stiffness. In higher frequency range, complex stiffness characteristic of HDM is dominated by volumetric stiffness of upper chamber and equivalent piston area [19], thus the

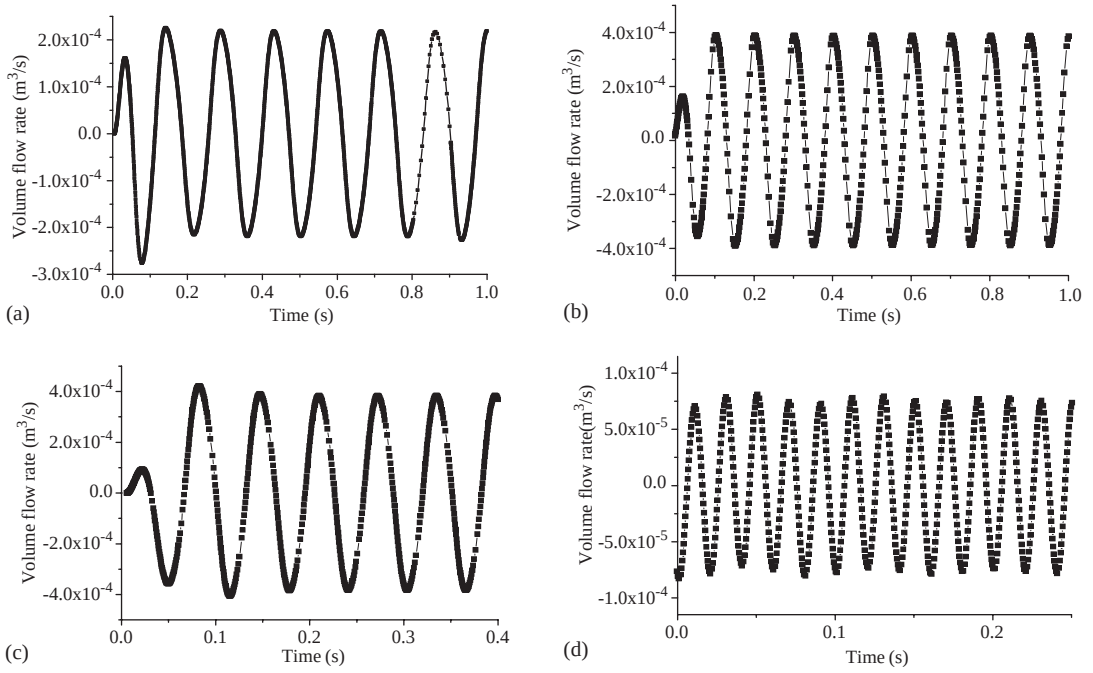

Fig. 17. Predicted results of volume flow rate through fluid track under preload of 800 N and harmonic excitation amplitude of 1 mm. (a) Frequency of 7 Hz, (b) frequency of 10 Hz, (c) frequency of 16 Hz, (d) frequency of 50 Hz.

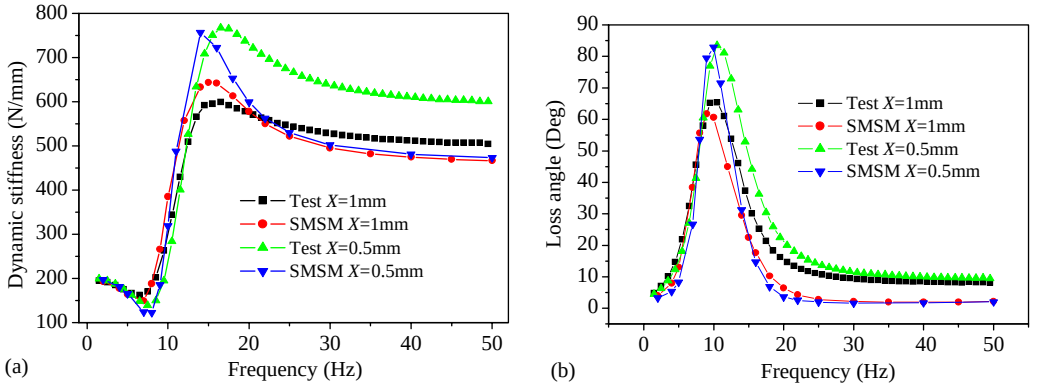

Fig. 18. Comparisons of analyzed and experimental results of dynamic stiffness and loss angle under preload of 800 N. (a) Dynamic stiffness, (b) loss angle.

identification accuracy of volumetric stiffness of upper chamber and equivalent piston area are essential to the prediction accuracy of dynamic stiffness and loss angle. In the presented dynamic characteristic simulation method, the adopted parameter identifications of volumetric stiffness and equivalent piston area only involve in static characteristics, therefore, more accurate parameter identifications of volumetric stiffness and equivalent piston area considering the frequency- and amplitude-dependent dynamic characteristic between chamber fluid and rubber

spring should be investigated to improve accuracy of predicted performance of HDM in the high frequency range. On the whole, the proposed modeling and simulation method is proved to be effective for isolation performance analysis of HDM particularly in low frequency range and around 10 Hz of resonance frequency of inertia track subsystem.

6. Conclusion

In this paper, a graphic modeling and simulation method of HDM is presented, which provides a convenient approach for characteristic analysis and prediction of HDM. The graphic model can be set up on effort–flow structure by attaching element units according to a systematic modeling procedure for multi-domain system, and automatic simulation can be carried out by the block-based numerical computation of Simulink. Moreover, parameter identifications using FE method for hyperelastic material, FE method for hydrostatic fluid–structure interaction and experimental analysis are carried out, which are integrated into the proposed graphic model of HDM. Investigations into static elasticity, dynamic characteristic and frequency response analysis of a typical HDM with fixed decoupler verify the effectiveness and practicability of the proposed method. This elementary characteristic simulation method of HDM is a practical and time saving method to computer-aided engineering system of HDM and PMS. In the future research, parameter identification methods of rubber viscoelasticity, dynamic FE analysis of rubber spring and identification method of chamber volumetric elasticity considering frequency- and amplitude-dependent characteristics should be investigated to improve accuracy of parameter identification for performance simulation of HDM in high frequency range.

Acknowledgement

The authors would like to thank Professor Zhen-Hua LU of Department of Automotive Engineering, Tsinghua University, PR of China for his advice and support in experimental and characteristic simulation of HDM. The authors would also like to thank Wuxi Csi vibration isolators Co., LTD, China for its assistance in testing HDM.

References

[1] R. Singh, G. Kim, P.V. Ravindra, Linear analysis of automotive hydro-mechanical mount with emphasis on decoupler characteristics, *Journal of Sound and Vibration* 158 (1992) 219–243.
[2] G. Kim, R. Sigh, Nonlinear analysis of automotive hydraulic engine mount, *Transaction of ASME, Journal of Dynamic Systems, Measurement, and Control* 115 (1993) 482–487.
[3] S.J. Gau, J.D. Cooton, Experimental study and modeling of hydraulic mount and engine system, SAE 951348.
[4] K. Holzemer, Theorie der gummilager mit hydraulischer dampfung, *ATZ* 87 (1985) 545–551.
[5] G. Kern, T. Grobmann, D. Gohilich, Computerunterstutzte auslegung von hydraulisch gedampften gummilagern, *ATZ* 94 (1992) 462–472.
[6] T. Sugino, E. Abe, Optimum application for hydroelastic engine mount, SAE 861412.
[7] K. Seto, K. Sawatar, Optimum design method for hydraulic engine mounts, SAE 911055.

[8] R.M. Brach, A.G. Haddow, On the dynamic response of hydraulic engine mounts, SAE 931321.
[9] W.C. Flower, Understanding hydraulic mounts for improved vehicle noise, vibration and ride qualities, SAE 850975.
[10] J.E. Colgate, C.-T. Chang, Y.-C. Chiou, W.K. Liu, L.M. Keer, Modeling of a hydraulic engine mount focusing on response to sinusoidal and composite excitations, *Journal of Sound and Vibration* 184 (1995) 503–528.
[11] P.L. Graf, R. Shoureshi, Modeling and implementation of semi-active hydraulic engine mounts, *Transactions of the ASME, Journal of Dynamic Systems, Measurement, and Control* 110 (1988) 422–429.
[12] K.H. Lee, Y.T. Choi, Performance analysis of hydraulic engine mount by using bond graph method, SAE 951347.
[13] L.R. Wang, J.C. Wang, I. Hagiwara, Modeling approach of functional model for multi-domain system, *JSME International Journal* Series C 48 (2005) No. 1.
[14] R.C. Rosenberg, D.C. Karnopp, *Introduction to Physical System Dynamics*, McGraw-Hill Book Company, New York, 1983.
[15] Matlab Manual version 6.1 release 12.1, Simulink: model based and system based design, The Mathworks Inc., USA, 2001.
[16] T. Shibayama, Y. Takashima, T. Horioka, Theoretical investigation of the dynamic characteristic of hydraulic mount, JSAE 9833278.
[17] L.R. Wang, Z.H. LU, Finite element simulation based modeling method for constitutive law of rubber hyperelasticity, *Rubber Chemistry and Technology* 76 (2003) 270–284.
[18] L.R. Wang, Z.H. LU, I. Hagiwara, Finite element simulation of static characteristics of vehicle rubber mount. *Proceedings of the I MECH Part D, Journal of Automobile Engineering* 216 (2002) 965–973.
[19] L.R. Wang, Study of Theory and Methods for Simulation of Nonlinear Characteristics of Hydraulically Damped Rubber Mount, PhD Thesis, Tsinghua University, Beijing, PR China, 2002.
[20] R.W. Fox, A.T. Mcdonald, *Introduction to Fluid Mechanics*, third ed., Wiley, New York, 1985.
[21] Y.Z. Li, M.S. Fan, *Fluid Mechanics*, High Education Press, Beijing, 1998.